Global Biogeochemical Cycles

RESEARCH ARTICLE
10.1029/2019GB006486

Sedimentary Nutrient Supply in Productive Hot Spots off the West Antarctic Peninsula Revealed by Silicon Isotopes

Lucie Cassarino[1], Katharine R. Hendry[1], Sian F. Henley[2], Ellen MacDonald[3], Sandra Arndt[4], Felipe S. Freitas[1], Jennifer Pike[5], and Yvonne L. Firing[6]

[1]School of Earth Sciences, University of Bristol, Bristol, UK, [2]School of Geosciences, University of Edinburgh, Edinburgh, UK, [3]School of Geographical and Earth Sciences, University of Glasgow, Glasgow, UK, [4]BGeosys, Biogeochemistry and Modelling of the Earth System, Department of Geosciences, Environment and Society Faculty of Sciences, Université Libre de Bruxelles, Brussels, Belgium, [5]School of Earth and ocean Sciences, Cardiff University, Cardiff, UK, [6]National Oceanography Centre, Southampton, UK

Key Points:
- Dissolved silicon fluxes from marine sediment along the West Antarctic Peninsula continental shelf are reported for the first time
- The silicon isotopic composition of porewater is used to assess diagenetic processes and the silicon budget at the sediment-water interface
- We find no clear evidence of a significant source of silicon from marine sediment along the West Antarctic Peninsula continental shelf

Supporting Information:
- Supporting Information S1

Correspondence to:
L. Cassarino,
l.cassarino@bristol.ac.uk

Citation:
Cassarino, L., Hendry, K. R., Henley, S. F., MacDonald, E., Arndt, S., Freitas, F. S., et al. (2020). Sedimentary nutrient supply in productive hot spots off the West Antarctic Peninsula revealed by silicon isotopes. *Global Biogeochemical Cycles*, *34*, e2019GB006486. https://doi.org/10.1029/2019GB006486

Received 26 NOV 2019
Accepted 23 NOV 2020
Accepted article online 17 DEC 2020

©2020. The Authors.
This is an open access article under the terms of the Creative Commons Attribution License, which permits use, distribution and reproduction in any medium, provided the original work is properly cited.

Abstract In this study we evaluate the benthic fluxes of silicic acid along the West Antarctic Peninsula (WAP). Silicic acid (DSi) is one of the macronutrients essential in fuelling biological hot spots of diatom-dominated primary production along the WAP. Here we measure the concentration and stable silicon isotopic composition of DSi in porewater profiles, biogenic silica content (BSi), and diatom abundance from sediment cores collected along the WAP. We couple these measurements with reaction-transport modeling, to assess the DSi flux and the processes that release this key nutrient from the sediment into the overlying waters. Our results show that the benthic DSi flux is dominated by the diffusive flux, which is estimated to be equivalent to 26.7 ± 2.7 Gmol yr^{-1} for the WAP continental shelf. The DSi isotope profiles reveal the important impact of sedimentary processes on porewater DSi and suggest that biogenic silica dissolution is the main source of DSi in porewaters and consequently of the benthic fluxes. Our integrated data-model assessment highlights the impact of surface productivity on sedimentary processes and the dynamic environment of core-top sediments where dissolution and reverse weathering reactions control DSi exchanges.

Plain Language Summary The West Antarctic Peninsula (WAP) is a highly productive region dominated by siliceous algae, diatoms. Biomass distribution is patchy along the WAP, and these hot spots are potentially enhanced by essential nutrients, that is, dissolved silicon, released from shallow marine sediments. We use observations of porewater concentrations and isotopes to show that the dissolved silicon flux from the sediments before the major diatom bloom period is low compared to the open Southern Ocean. However, both our observations and modeling reveal a strong link between surface water uptake and sedimentary release of dissolved silicon, such that benthic fluxes will increase during the summer season. We predict a significant variability in benthic silicon flux, tied to diatom productivity, which is highly sensitive to climatically driven changes in sea ice dynamics.

1. Introduction

The West Antarctic Peninsula (WAP) is characterized by high algal production during the austral summer months, which supplies organic matter to support a rich ecosystem that contributes to a substantial sequestration of carbon (Barnes, 2018). The WAP is also one of the most climatically sensitive regions on Earth, experiencing extreme seasonal changes as well as interannual variability driven by atmospheric and oceanic forcing (Meredith et al., 2017), superimposed on longer-term climate and ocean warming (Henley et al., 2019; Hobbs et al., 2016; Turner et al., 2016). The highly dynamic sea ice cycle along the WAP causes oceanographic conditions—and so light, nutrient, and grazing conditions—to vary over fine spatial and temporal scales resulting in highly heterogeneous production concentrated in biological hot spots (Kohut et al., 2018; Schofield et al., 2013; Venables et al., 2013). However, the specific mechanisms behind the location and extent of these hot spots, and so the productivity and storage of organic carbon, are not fully understood.

One of the key drivers of production is nutrients supplied by upwelling deep waters. The Antarctic Circumpolar Current (ACC), flowing around the continent, is bathymetrically constrained by the narrow Drake Passage and forced to flow along the WAP near the shelf break (Orsi et al., 1995) facilitating transport of warm, nutrient-rich Circumpolar Deep Water (CDW) onto the WAP shelf by processes including eddies, upwelling, and interaction with topography through glacially carved canyons crosscutting the shelf (Couto et al., 2017; Martinson & McKee, 2012; Martinson et al., 2008; Moffat & Meredith, 2018; Venables et al., 2017). In the process, CDW is modified (producing modified CDW, mCDW) by mixing with the cold, fresher surface water (Couto et al., 2017). High concentrations of surface chlorophyll observed in the vicinity of submarine channels led to the canyon hypothesis, which states that upwelling mCDW funneled through and up the canyons leads to the patchy supply of heat and nutrients to the surface and thus the heterogeneous nature of WAP primary production within the coastal fjords (Kavanaugh et al., 2015; Schofield et al., 2013). A recent high-frequency radar study, however, suggested that the period of growth of phytoplankton is longer than their residence time within such hot spots, suggesting that algal cells are concentrated in these regions by advection rather than growing in situ (Kohut et al., 2018). On a seasonal to interannual time scale, the duration of sea ice cover is the key variable that controls water column stratification (Brearley et al., 2017) that strongly impacts primary productivity due to the stability of the light to which phytoplankton are exposed and by controlling nutrient supply from deeper waters to the surface layer, which drives phytoplankton bloom strength and duration.

Macronutrient concentrations (nitrate, phosphate, and silicic acid denoted by dissolved silicon (DSi), that is, $Si(OH)_4$), are high in CDW, and there is evidence from combined transects of water column nutrient profiles (Henley et al., 2018) for greater DSi enrichment from the sediment relative to other nutrients. This enrichment, if transferred vertically to the water column and into the productive fjords, could have major implications for algal community composition by promoting diatom growth relative to other groups (Henley et al., 2018). However, the rate of DSi input from the sediments, and the early diagenetic mechanisms behind the flux, is not constrained. The WAP is characterized as a "high recycling, low export" area where most of the biogenic silica (BSi) produced by diatoms that sinks out of the photic zone will remineralize and release DSi back into the water column, with BSi export ranging from 0.3% to 10% of surface production on the continental shelf (Buesseler et al., 2010). The BSi that reaches the seafloor undergoes early diagenetic in the upper sediment layers, principally dissolution or formation of authigenic solid phases (so-called reverse weathering) during burial, supplying DSi to the porewaters or exchanging Si between dissolved and particulate phases (Aller, 2014; McManus et al., 1995; Van Cappellen & Qiu, 1997). Such complex behavior means that the sources of the DSi fluxes cannot be determined from concentration measurements alone.

The stable silicon isotopic composition ($\delta^{30}Si$) of natural materials is a powerful tool for tracing physical, chemical, and biological reactions, due to the preferential uptake or release of the lighter isotope that results in isotopic fractionation. The geochemical impacts of diagenetic processes such as the formation of secondary phases have been shown to be reflected in profiles of the $\delta^{30}Si$ of porewater DSi ($\delta^{30}Si_{DSi}$) profiles (i.e., Ehlert et al., 2016; Geilert et al., 2020; Ziegler et al., 2005). Authigenic clay formation leads to the enrichment of the heavier silicon isotopes ^{29}Si, ^{30}Si in solution, due to the preferential precipitation of the light isotope in the solid phase (Ehlert et al., 2016; Georg et al., 2009). Unlike for authigenic precipitation, Si isotopic fractionation during dissolution is still an open question. To date, two laboratory-based experiments have demonstrated contradictory results, showing either that the lighter isotopes are preferentially released from BSi, leading to a lower $\delta^{30}Si_{DSi}$ signature in the solution (−0.55 ‰) (Demarest et al., 2009), or that there is no fractionation at all and thus dissolution of diatoms will release DSi with a similar isotopic composition to the diatom frustules (Wetzel et al., 2014).

Here, we use various approaches to investigate the flux of DSi from the shelf sediments at three locations along the WAP. We investigate both the pelagic component, using water samples from the full water column depth and the benthic system, through downcore sediment and porewater analyses. We use bottom water and porewater depth profiles of both DSi concentrations and stable silicon isotopic compositions to assess the DSi benthic flux to the bottom waters. DSi concentrations and Si isotopic compositions from the water column and porewaters, together with sedimentary BSi concentrations and diatom abundance, and major and trace element concentrations in sediments are used to evaluate the processes that release this key nutrient from WAP shelf sediments. We have combined these empirical results with a number of modeling approaches, including isotope mass balance calculations and a reaction-transport model. Together, data

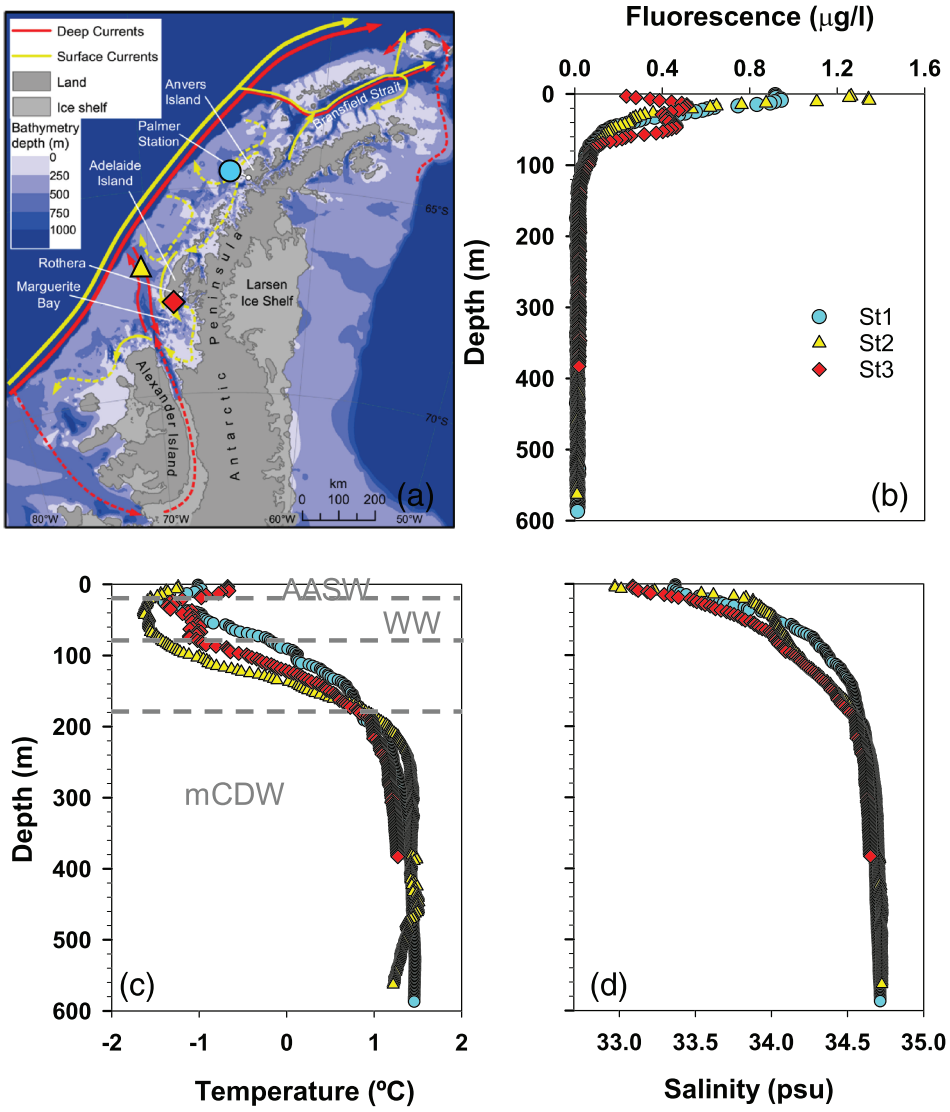

Figure 1. Sample location and oceanographic context along the West Antarctic Peninsula. (a) Map of the West Antarctic Peninsula with arrows showing surface and deep ocean circulation and location of JR15003 sampling Station 1 (blue circle), Station 2 (yellow triangle), and Station 3 (red diamond). Map adapted from Meredith et al. (2017). (b) Fluorescence profile at the three stations (NB: concentration measured at the beginning of the ice-free season meaning they are not being representative of midsummer, they are quantitative but uncalibrated. (c) Temperature and (d) salinity of seawater with the deep saline and warm modified Circumpolar Deep Water (mCDW) overlayed by the Winter Water (WW) and the Antarctic Surface Water (AASW).

and model results highlight the dissolution/precipitation control on sedimentary DSi concentrations and the potential use of $\delta^{30}Si_{DSi}$ in the porewaters as a proxy for early diagenesis.

2. Methods

2.1. Sampling Area and Methods

Seawater was collected by Niskin bottles attached to the CTD rosette, and sediments and porewaters by box coring, at Stations 1, 2, and 3 along the WAP (Figure 1) at the beginning of the ice-free season, between 25 and 28 December 2015. Temperature, salinity, and fluorescence were recorded during the entire CTD cast, and the reported values are the average of the downcast and upcast. Seawater samples were collected on the upcast.

Seawater samples were filtered through 0.2 μm filters and stored at 4°C for DSi analysis and −18°C for nitrate, nitrite, phosphate, and ammonium analyses in acid-cleaned (2N reagent grade HCl) polypropylene

bottles. For the sediment samples, two cores were sampled during each box coring event. The first core was sliced every 2 cm for sediment analysis, and the second core was reserved for porewaters, sampled by Rhizons (Rhizosphere) with a resolution of 2 cm. Samples for DSi, BSi, and Si isotopes were analyzed at the Bristol Isotope Group Facility, University of Bristol, and X-ray fluorescence (XRF) analyses were carried out at the School of Geosciences, University of Edinburgh.

2.2. DSi, BSi, and $\delta^{30}Si_{DSi}$ Analysis

DSi analysis of seawater and porewater samples was carried out using Hach Lange spectrophotometer with the Heteropoly Blue Method, which follows Strickland and Parsons (1972).

BSi was determined by alkaline extraction following the method from DeMaster (1981) and Hawkings et al. (2017). Approximately 30 mg of dry sediment was accurately weighed with 50 ml 0.985 M Na_2CO_3 solution added and heated at 85°C. One milliliter aliquot was sampled after 2, 3, and 5 hr and kept overnight at 4°C to stop further dissolution. BSi analysis was carried out by the automatic flow injection analysis (FIA) in Bristol Glaciology Centre, School of Geographical Sciences, University of Bristol. The precision, 0.65%, and accuracy, 2.6%, were determined by external standard measurements. For $\delta^{30}Si$ analysis, silicon was first coprecipitated following the MAGIC method from Karl and Tien (1992) with Reynolds et al. (2006) modification. Samples were purified by cation exchange chromatography and $\delta^{30}Si_{DSi}$ analysis was carried out at Bristol on the MC-ICP-MS (Multi-Collector Inductively-Coupled-Plasma Mass-Spectrometer, Finnigan Neptune s/n 1002, Bristol Isotopic Group). All sample analyses were replicated ($n \geq 2$) and followed the typical standard-sample bracketing and Mg doping from Cardinal et al. (2003). The $\delta^{30}Si_{DSi}$ results are reported relative to the standard NBS28 following Equation 1.

$$\delta^{x}\mathrm{Si}(‰) = \left(\frac{\left(\frac{^{x}\mathrm{Si}}{^{28}\mathrm{Si}}\right)_{sample}}{\left(\frac{^{x}\mathrm{Si}}{^{28}\mathrm{Si}}\right)_{standard}} - 1 \right) \quad (1)$$

with x corresponding to ^{29}Si or ^{30}Si and the standard being the international Si standard Quartz NBS28 (RM8546).

External reproducibility was assessed by repeated measurement of the biogenic opal standard, LMG-08 (Hendry et al., 2011), with a mean value of −3.45 ‰ and a reproducibility of the repeated measurement of ±0.17 ‰ (2 s.d.) corresponding to the uncertainty interval of all $\delta^{30}Si$ data in this study. The new seawater standard ALOHA deep was analyzed as an additional quality check and yielded values within error of those obtained during an interlaboratory study (Grasse et al., 2017): $\delta^{30}Si = 1.11 \pm 0.18$ ‰ and $\delta^{29}Si = 0.57 \pm 0.12$ ‰ (2 s.d, $n = 10$). Our results fit with the published standard values with LMG-08: $\delta^{30}Si = -3.37 \pm 0.17$ ‰ (2 s.d.) (Hendry et al., 2011) and ALOHA deep: $\delta^{30}Si = 1.24 \pm 0.20$ ‰ and $\delta^{29}Si = 0.65 \pm 0.10$ ‰ (2 s.d.) (Grasse et al., 2017). For all samples and standards, the three isotopes (^{28}Si, ^{29}Si, and ^{30}Si) were measured and results show good agreement with the mass-dependent fraction between $\delta^{29}Si$ and $\delta^{30}Si$ with $\delta^{29}Si = 0.509\ \delta^{30}Si$.

2.3. Diffusive Benthic Fluxes

The diffusive DSi flux across the sediment-water interface can be defined using different methods: deployment of benthic chambers, core-incubation, and calculation based on concentration gradients derived from porewater DSi profiles. Here, benthic chambers deployment and core incubations were not possible, so the diffusive fluxes were calculated based on the concentration gradient in the uppermost layer of the sediment cores. Porewater DSi profiles can be used to calculate the diffusive flux with reduced uncertainties by fitting an idealized, nonlinear concentration curve to the data to obtain a concentration gradient across the sediment-water interface (Ragueneau et al., 2000). However, such curve fitting is challenging in this study as the porewater DSi concentrations do not display the typical asymptotic increase with depth, in particular at Station 2. Instead, we use a two-point calculation method following Fick's first law of diffusion (Equation 2). To test the sensitivity of the flux estimates based on the concentration gradient using two points, we compared the use of (i) the deepest Niskin bottle sampled during CTD casts and (ii) core-top water as end-member values for bottom water.

The diffusive DSi flux across the sediment-water interface (J_{sed}) was defined according to the Fick's first law of diffusion by Equation 2,

$$J_{sed} = -\phi \cdot D_{sed} \cdot \frac{\partial C}{\partial x} \quad (2)$$

$$D_{sed} = \frac{D_{sw}}{1 - \ln(\phi^2)} \quad (3)$$

where ϕ is the sediment porosity, D_{sed} is the diffusion coefficient of DSi corrected for tortuosity (Boudreau, 1996) (Equation 3), D_{sw} is the diffusion coefficient of DSi in seawater ($D_{sw} = 4.7{\cdot}10^{-10} \pm 0.01{\cdot}10^{-10}$ m^2 s^{-1} for $T = 2$°C Rebreanu et al., 2008). $\partial C/\partial x$ is the DSi concentration gradient between two points; porewater (2 cm deep in the sediment) and bottom water estimated from (i) the deepest Niskin bottle sampled during CTD casts (10 m above the seafloor) and (ii) core-top water (50 cm above the sediment sampled from the box core) (as listed in Table S1 in the supporting information [SI]).

2.4. Diatom Assemblage Analysis

Samples for diatom analysis were prepared and analyzed at Cardiff University and the University of Bristol. Microscope slides for quantitative diatom assemblage analysis were prepared following a standard acid cleaning and settling method (Scherer, 1994). Slides were analyzed using phase contrast light microscopy at 1,000X magnification. Rarefraction tests indicated that a minimum of 600 valves were required to capture the full diatom diversity so slides were systematically traversed until 600 valves had been counted. Counting followed the procedure of Schrader and Gersonde (1978). In all cases, diatoms were identified to species. Long, pennate taxa such as *Thalassiothrix* and *Trichotoxon* were counted as 0.5 when one pole was present. For the core from St1, a second CRS-free count was conducted (400 valves) to elucidate smaller environmental signals. Relative diatom species abundances were calculated as a percentage of the total diatom assemblage for each slide. Absolute diatom abundance (diatoms per gram of sediment) was calculated using the following equation from Scherer (1994): $T = (N\,B)/(AF)/M$, where T is the number of diatoms per grams, N the total number of diatoms counted, B the area of bottom of settling beaker (mm^2), A the area per field of view (mm^2), F the number of fields of view counted, and M the mass of the sample (g). Further details are given in the SI.

2.5. XRF Analysis and Cations

Major element concentrations were measured on fused glass disks prepared by a method similar to Norrish and Hutton (1969). Samples were dried at 110°C overnight to remove adsorbed moisture then homogenized and ignited at 1100°C to decompose carbonates and hydrous silicates. The 0.95 g aliquots of dried, unfired sample was then weighed into Pt95Au10 crucibles and mixed thoroughly with borate flux (Johnson and Mathey Spectroflux 105) in a 1:5 sample:flux ratio. This mixture was fused at 1100°C for 20 min in a muffle furnace then cooled to room temperature to form a glass. After fusion, mass lost due to devolatilization of hydrous silicates and carbonates was replaced with additional flux to regain the initial 5:1 sample:flux ratio. Samples were then fused for a second time over a Meker burner being swirled thoroughly to ensure homogeneity. The molten mixture was poured onto a graphite plate and formed into a glass disk by compression using an aluminum plunger at 220°C. The samples were analyzed on a Philip PW2404 XRF spectrometer using a Rh tube for the primary radiation. The instrument was calibrated using 20 internationally recognized standard materials (Govindaraju, 1994). Line overlap factors were calculated using these international standards, with major element corrections being applied for Ca on Mg, Ti and P, and Mg on Na.

Potassium cations concentration of porewaters were measured by inductively coupled plasma-optical emission spectrometry (ICP-OES Agilent 710 simultaneous spectrometer) at the Aqueous Geochemistry facilities of the University of Bristol.

2.6. Age Model

^{210}Pb analyses were carried out at GAU-Radioanalytical Laboratories, National Oceanography Centre, Southampton. The samples were measured by alpha spectrometry of ^{210}Po, a proxy method that gives the activity of ^{210}Pb, as ^{210}Po is a granddaughter of ^{210}Pb (Appleby, 2008). The sediment samples were almost 2 yr old for ^{210}Pb analysis so it is assumed ^{210}Pb had reached secular equilibrium with ^{210}Po (half-life = 138 days) within the sediment (Baskaran, 2011; San Miguel et al., 2002).

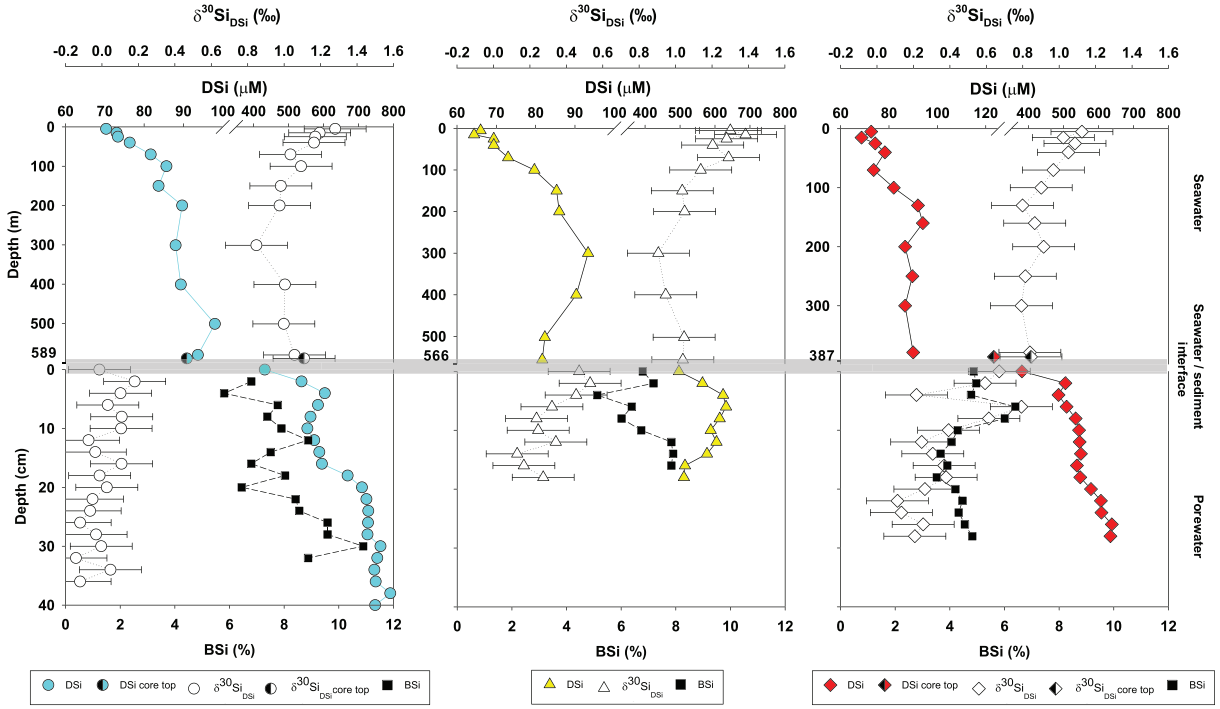

Figure 2. Silicic acid (DSi, colored symbols), silicon isotopes of DSi ($\delta^{30}Si_{DSi}$, open symbols), and biogenic silica (BSi, black squares) profiles of seawater (upper panel), porewaters/sediment (lower panel), and core-top water (half-filled) along the West Antarctic Peninsula. From north to south, St1 (blue circles) with the deepest water depth corresponding to 589 m, St2 (yellow triangles) with water depth = 566 m, and St3 (red diamonds) the shallowest with water depth = 387 m. Core-top data point of St1 and St3 profile corresponds to seawater sampled 50 cm above sediment. NB: the scale for the water column is in meters and for the sediment in centimeters. The gray bar represents the water/sediment interface. $\delta^{30}Si_{DSi}$ error bars represent external error, 0.17 ‰ (2 s.d.).

3. Results

3.1. Oceanographic Context of the WAP

Temperature and salinity profiles along the WAP show a strong stratification in the top 100 m where temperature decreases and salinity increases with depth (Figures 1c and 1d). The mCDW in the bottom layer is characterized by higher temperature and higher salinity and is overlain by remnant Winter Water (WW), which exhibits negative temperatures and lower salinity with an average depth of ~70 m, based on data from the Rothera Time-series (RaTS) (Venables et al., 2013). Station 2 shows the coldest near-surface temperature (of −1.6°C), likely due to lateral mixing of cold water by surface currents.

3.2. Seawater DSi and Silicon Isotope Profiles

Seawater DSi concentrations at the three stations along the WAP (Figure 2) exhibit a nutrient-like profile with lower concentrations (66–72.7 μM) in surface water, due to surface productivity, and higher concentration in the subsurface, caused by remineralization of sinking particles. These higher concentrations range from 79.7 μM (Station 1, St1) to 89.7 μM (Station 2, St2), where they are found between 100 and 200 m, whereas Station 3 (St3) shows a shallower gradient with a remineralization depth at 40 m. The extent of DSi surface drawdown agrees with the fluorescence-derived chlorophyll concentrations indicating the highest biological activity at St2 and lowest at St3. The fluorescence peak at St3 is located at approximately 15 m (Figure 1b), similar to the maximum chlorophyll concentration observed at the RaTS site, also within Ryder Bay (Clarke et al., 2008). Sampling took place prior to the peak of the phytoplankton bloom; therefore, our fluorescence measurements cannot be used to infer midsummer conditions at the WAP. Seawater DSi concentration peaks at 500 m for St1, 300 m for St2 and 200 m for St3, showing the progressive intrusion and shoaling of nutrient-rich mCDW along the WAP.

Due to the preferential biological uptake of light isotopes, $\delta^{30}Si_{DSi}$ profiles in seawater are negatively correlated with DSi, with heavier $\delta^{30}Si_{DSi}$ at the surface ranging between 1.03 ± 0.17 ‰ (2 s.d., external error for all $\delta^{30}Si_{DSi}$ measurements, see section 2) and 1.30 ‰. $\delta^{30}Si_{DSi}$ profiles decrease with depth reaching the lightest $\delta^{30}Si_{DSi}$ at 300 m for all three stations, showing the intrusion of mCDW. The less modified water at St1

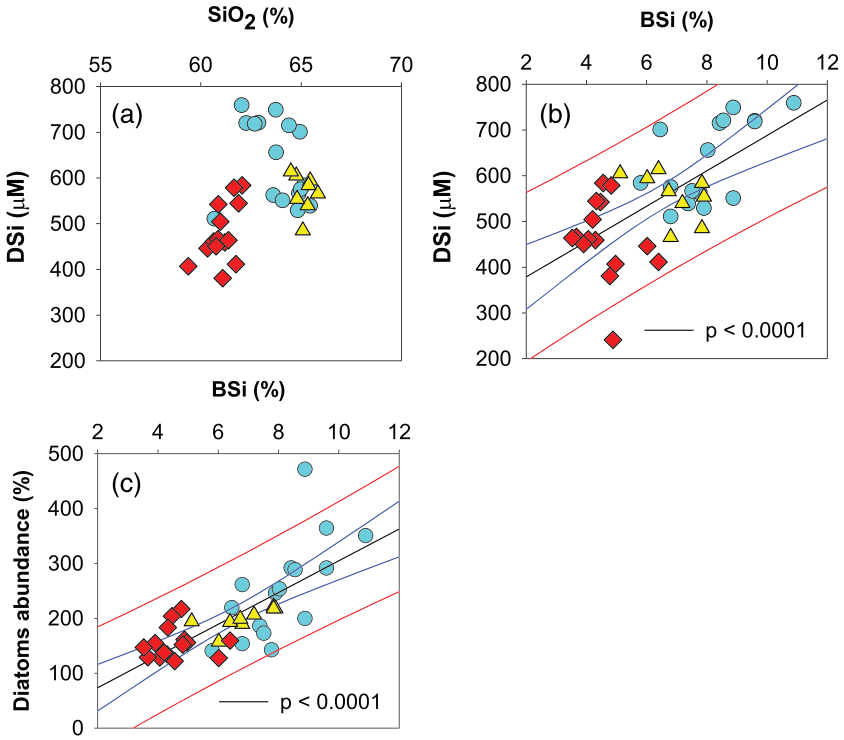

Figure 3. Silicic acid (DSi) against (a) total silicate (SiO_2) (not significant), (b) biogenic silica (BSi), and (c) diatom abundance against BSi content with linear regression (black line), the 95% confidence interval (blue lines) and the 95% prediction interval showing the significant relation (p <0.05) between DSi and BSi, and diatom abundance and BSi.

has an observed $\delta^{30}Si_{DSi}$ = 1.00 ‰, in accordance with previous Upper Circumpolar Deep Water (UCDW) measurements from Hendry, Georg, et al. (2010), while lower values at St2 and St3 of $\delta^{30}Si_{DSi}$ = 0.91 ‰ are similar to measured mCDW in Marguerite Bay (Annett et al., 2017).

3.3. Porewaters and Sediments

DSi concentrations in porewaters do not follow the typical asymptotic DSi profile (Aller, 2014), but they show a relatively sharp gradient at the surface sediment, from around 400 µM at 0 cm to 600 µM at 6 cm, and a slower increase in deeper layers, except for a decrease below 8 cm at St2 and another sharp increase from 16 to 20 cm at St1 (Figure 2).

Si isotopic composition of DSi in porewaters ($\delta^{30}Si_{DSi\ pw}$) shows a general negative correlation with DSi profiles ($\delta^{30}Si_{DSi\ pw} = -0.002$ DSi + 0.98, $r^2 = 0.46$, $p < 0.0001$) and is isotopically lighter than the $\delta^{30}Si_{DSi}$ of the bottom water at all stations (Figure 2). For all the stations $\delta^{30}Si_{DSi\ pw}$ gets lighter with depth. St1 shows the least variable $\delta^{30}Si_{DSi\ pw}$ profile (St1 $\delta^{30}Si_{DSi\ pw} = 0.01 \pm 0.17$ ‰ [2 s.d.]) compared to St2 (St2 $\delta^{30}Si_{DSi\ pw} = 0.32 \pm 0.27$ ‰ [2 s.d.]) and St3 (St3 $\delta^{30}Si_{DSi\ pw} = 0.37 \pm 0.41$ ‰ [2 s.d.]) (Figure 2).

BSi abundances at the three stations exhibit distinctive profiles, with positive and negative excursions at different depths (Figure 2). St1 shows a relative increase in BSi with depth from 6.8% to 10.9%. BSi content at St2 between 2 and 4 cm shows a sharp decrease, with an increase in the deeper layers, and stabilizes at 14%cm; its BSi content varies between 5.1% and 7.9%. St3 exhibits a nearly constant BSi content of around 4.3% except at 6 and 8 cm where it reaches 6.4% (Figure 2).

Diatom abundance, expressed as diatoms per gram of sediment, has a statistically significant linear relationship with BSi (Diat = 28.91 BSi + 15.87, r^2 = 0.54, p <0.0001, Figure 3c), indicating that our BSi is predominantly yielded by diatoms rather than lithogenic material or abiological amorphous precipitates. Species and abundance are shown and described in the SI (Figure S1).

The marine sediments of our study are composed of fine-grained opal and clay. The XRF data show that SiO_2 content of the sediment ranges between 59.3% and 65.8%, with Al_2O_3 = 11.5–15.4%, Fe_2O_3 = 5.3–6.8%,

Table 1
Comparison of Benthic Fluxes at the Three Stations Along the WAP Using Deepest CTD or Core-Top Water as the Nutrient End-Member

∂C/∂x		J_{sed} (mol m^{-2} yr^{-1})
Deepest CTD/porewater	Station 1	$2.03 \cdot 10^{-4}$
	Station 2	$3.75 \cdot 10^{-4}$
	Station 3	$2.39 \cdot 10^{-4}$
Core top/porewater	Station 1	$9.24 \cdot 10^{-2}$
	Station 2	n.d.
	Station 3	$8.59 \cdot 10^{-2}$

Note. ∂C/∂x = gradient between deepest CTD Niskin sample or core-top water and DSi in porewater. n.d. = not determined.

MgO = 2.8–3.6%, Na_2O = 3.3–6.2%, and K_2O = 1.6–2.5% (details are presented in Table S2 in the SI) indicating a composition dominated by montmorillonite-type detrital clay minerals.

The ^{210}Pb measurements show that the sedimentation rates at the core locations range from 1.53 to 2.15 mm yr^{-1}, which is in agreement with previous observations (Smith et al., 1999).

The potassium (K^+) concentration profiles of the porewaters range between 15.8 and 18.38 mM (Figure S2 in the SI). It is clearer in Figure 5d that K^+ is positively correlated with DSi ($K^+ = 0.003$ DSi + 15.6, $r^2 = 0.28$, $p < 0.001$) and negatively correlated with $\delta^{30}Si_{DSi\ pw}$ ($\delta^{30}Si_{DSi\ pw} = -0.24\ K^+ + 4.3$, $r^2 = 0.46$, $p < 0.00001$).

Our results suggest that at our three sites along the WAP the porewater and the sediment are not in steady state and indicate that porewater respond to BSi dissolution and precipitation of authigenic phase. The lack of steady state is likely a result of the high sedimentation rate and the highly dynamic nature of BSi export in this region, which will be important drivers of sedimentary Si cycling.

3.4. Diffusive Benthic Fluxes of DSi

The steady-state benthic fluxes, denoted by J_{sed}, are estimated from Fick's first law of diffusion (Equation 2) and assuming molecular diffusion of DSi across the concentration gradient at the sediment-water interface (Schulz & Zabel, 2006). Table 1 shows the DSi diffusive fluxes obtained by using the deepest CTD water depth sample and the core-top water as end-members of the concentration gradient. No comparison is available for St2 due to the lack of a core-top water sample. Our results show a difference of 2 orders of magnitude between the two gradients. The examination of the limitations of the two-point calculation and the choice of the core-top/porewater gradient as our representative diffusive flux can be found in the discussion section 4.1.1.

4. Discussion

4.1. Benthic Fluxes and Si Budget From WAP Sediments

4.1.1. Diffusive Fluxes of DSi and Limitations

The direct application of Fick's first law of diffusion to real-world data is often challenging for a number of reasons. First, the determination of ∂C/∂x is hampered by physical sampling constraints given that bottom water sampling by Niskin bottle (5–20 m distance from the seafloor) will not capture the concentrations of the nutrient in question within the boundary layer. At our stations, we were able to compare the bottom water sample from the deepest CTD Niskin samples (DSi_{ctd}) and the core-top water from the box corer ($DSi_{coretop}$). Data show that DSi_{ctd} and $DSi_{coretop}$ are similar for St1, in contrast to St3, where DSi_{ctd} is lower than $DSi_{coretop}$ (Figure 2). The significant difference in concentrations between the core top and deepest CTD samples raises the question of the accuracy of diffusive flux calculations based on Equation 3 in situation where true bottom water concentrations are not known. Table 1 shows that using our deepest CTD Niskin samples (approximately 10 m above the seafloor) produces diffusive fluxes 2 orders of magnitude smaller than using the core-top water sample (approximately 0.5 m above the seafloor). Hence, previous studies that used the niskin bottle values may have underestimated fluxes.

The second challenge is that the results are highly sensitive to the assumed value of the porosity. The sediment surface shows variability in porosity, with ϕ St1 = 0.6, ϕ St2 = 0.8, and ϕ St3 = 0.7 between 0 and 2 cm depths, all of which are in the range of the average porosity reported in this area (Volpi et al., 2003)

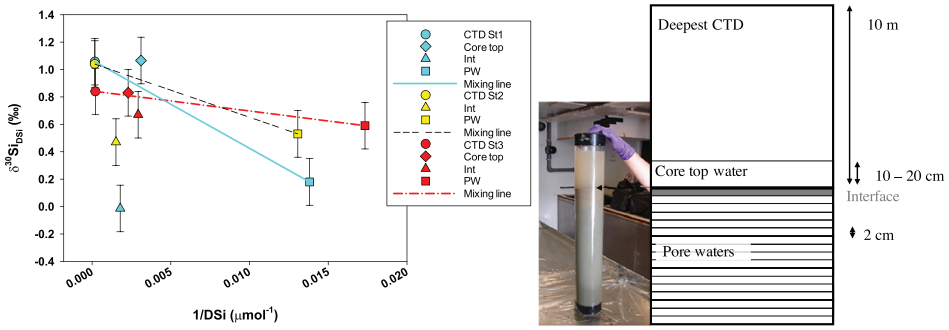

Figure 4. (left) $\delta^{30}Si_{DSi}$ against 1/DSi in μmol^{-1} for deepest CTD (circles), core-top water (diamonds), sediment-water interface (triangle), and porewater at 2 cm depth (square) of Station 1 (blue), Station 2 (yellow), and Station 3 (red). The lines represent the mixing line between the two end members: deepest CTD and porewater. Conservative mixing is indicated by the samples that fall on the linear mixing curve between the end-members. Loss or gain of Si to or from the porewaters and/or interface waters is indicated by a deviation from linearity. (right) Schematic showing the reservoir depth and scale difference.

(0.6 to 0.75). As such, the porosity of each site has been corrected with the mass of water expelled from sediment (M_p), the porewater density (ρ_w), and the wet bulk density (ρ_b) using Equation 4 following Brown and Ransom (1996) to better represent the site specific diffusive fluxes.

$$\phi = \left(\frac{M_p}{\rho_w}\right)\rho_b. \tag{4}$$

The benthic diffusive DSi flux values, 0.086 to 0.092 mol m^{-2} yr^{-1} (Table 1), when scaled up to the whole shelf area ($3{\cdot}10^{11}$ m^2, Ducklow et al., 2012) result in a flux of 26.7 ± 2.7 Gmol yr^{-1} (2 s.d) for the WAP continental shelf. These estimates are in the range of the open Atlantic and Arctic Oceans (0.001–0.117 mol m^{-2} yr^{-1}), but lower than estimates for continental slopes (0.17–2.01 mol m^{-2} yr^{-1}) and most open Southern Ocean regions (0.37–2.03 mol m^{-2} yr^{-1}) (see the SI for details). Our relatively low diffusive fluxes would have resulted from the time of sampling, given that the box coring occurred prior to the main bloom of the season, whereas higher fluxes may be expected after summer production has been exported to the seafloor during the autumn period (Ragueneau et al., 2001). Additionally, our calculations may be missing some very fine scale diffusive processes at the sediment-water interface (upper few millimeters of sediment), where most of the dissolution is likely to be occurring (Ragueneau et al., 2000). Most critically, these calculations consider only diffusion and neglect advective processes, bioturbation, bioirrigation, iceberg disturbance, brine injection, and resuspension by bottom water currents (Hendry, Meredith, et al., 2010; Venables et al., 2017), thus representing a minimum estimate for the region. Benthic chambers or core incubations can be employed to capture some of these processes (Berelson et al., 1997; Koning et al., 1997; Ragueneau et al., 2009; Sayles et al., 1996). However, in the highly dynamic WAP environment benthic chambers are logistically challenging to deploy for the periods of time that could describe a sufficiently integrated signal and are unlikely to capture key disturbances from strong currents and other physical perturbations. Instead, we can use our silicon isotope measurements as an additional constraint to carry out a simple mass balance calculation to investigate the proportion of the DSi in the mCDW that originates from the sediment flux. The low DSi fluxes from the WAP sediments might also come from the lower DSi gradient at the sediment water interface. Compared to the Arctic Ocean and the Open Southern Ocean, here the bottom water (i.e., mCDW) is rich in DSi (81.7–93.7 μM) meaning that the diffusion gradient is smaller than in the open ocean. Additionally, despite the contribution of BSi dissolution, our sediments are not located in the opal belt where sediments can be composed of 35% BSi (Rabouille et al., 1997) and in the Ross sea can range between 1% and 85% (DeMaster et al., 1996). Also, high DSi benthic fluxes have been reported in the Indian sector of the Permanently Open Ocean Zone (POOZ) area (Rabouille et al., 1997), which is also the area characterized by an overall opal preservation efficiency higher than the rest of the Southern Ocean (Pondaven et al., 2000).

4.1.2. Si Isotope Mass Balance Approach

It has been shown by Fripiat et al. (2011) and others (e.g., Annett et al., 2017; Cassarino et al., 2017) that seawater DSi and $\delta^{30}Si_{DSi}$ have a linear relationship that can be used as a mixing tracer between water masses. Here, we apply the same principle to the porewater data, considering the porewater at 2 cm depth as the

Table 2
Fractional Contribution of Porewater Toward the Deepest CTD Using Either the Interface or the Upper Sediment Water as Intermediate Layer and Si Budget

	Station 1	Station 2	Station 3
Fraction of Si (f, Equation 5) from:			
Interface	1.22	1.12	0.68
core top	−0.01	n.d.	0.04
Si Budget (mol m^{-2}):			
PW to core top	0.221	n.d.	0.151
core top to CTD	−0.03	n.d.	0.018

Note. All parameters used to calculate Si budget are summarized in the SI.

nutrient-rich end-member, the interface as the homogeneous intermediate reservoir, and the deepest CTD Niskin sample as the low-nutrient end-member.

In the condition of conservative mixing between two different source waters, intermediate reservoirs fall along a straight line between the end-members and it is possible to calculate the fractional contribution ($f_{A\ to\ B}$) of an end-member A to a reservoir B. Here only St3 is described by conservative mixing (Figure 4). The fractional contribution of the porewater to the interface at St3 can therefore be expressed as f_{P-I} (Equation 5):

$$f_{P-I} = \frac{\delta^{30}\mathrm{Si}_{\mathrm{DSi\ int}} - \delta^{30}\mathrm{Si}_{\mathrm{DSi\ ctd}}}{\delta^{30}\mathrm{Si}_{\mathrm{DSi\ pw}} - \delta^{30}\mathrm{Si}_{\mathrm{DSi\ ctd}}} \quad (5)$$

where $\delta^{30}\mathrm{Si}_{\mathrm{DSi\ int}}$, $\delta^{30}\mathrm{Si}_{\mathrm{DSi\ ctd}}$, and $\delta^{30}\mathrm{Si}_{\mathrm{DSi\ pw}}$ are the Si isotopic signature of the interface, deepest CTD water and porewater.

For both St1 and St2, the intermediate reservoirs do not fall on a simple mixing line; despite differences in DSi concentrations, the interface waters are isotopically similar to porewaters and the core-top waters are isotopically similar to seawater. This nonconservative behavior suggests that between the interface, the core-top water and the bottom water there is a loss of DSi due to a physical mechanism, rather than a chemical or biological reaction that would result in isotopic fractionation (Table 2). We suggest that the porewater isotopic signature is being retained in the interface but because of a relatively small amount of DSi-rich water coming out of the sediment compared to the vast seawater reservoir above, the sediment-derived DSi is being removed rapidly by advective processes. Furthermore, the effect of lateral mixing is likely to be smaller in a more quiescent environment such as St3 (Wallace et al., 2008), explaining the better fit to the mixing model at this station.

4.1.3. Where Is the DSi Coming From?

Our $\delta^{30}\mathrm{Si}_{\mathrm{DSi}}$ data show that there is a flux of DSi from the sediment into the overlying water, which is rapidly transported away and incorporated into mCDW. We can also use the DSi and $\delta^{30}\mathrm{Si}_{\mathrm{DSi\ pw}}$ data to explore the source of this DSi. Within shallow marine sediments, DSi is released either by dissolution of BSi (or other reactive phases) in undersaturated environments (DeMaster, 2013) or exchanged with solid phases as a result of coprecipitation with other elements such as aluminum (Al), iron (Fe), potassium (K), and magnesium (Mg), as well as authigenic mineral formation (Aller, 2014).

Here, three scenarios are envisaged for our sediment core sites. First, if BSi dissolution is the dominant process, it will be characterized by a decrease in BSi content coupled to an increase in DSi concentration and lighter $\delta^{30}\mathrm{Si}_{\mathrm{DSi\ pw}}$ with depth. The trend toward a lighter isotopic ratio would largely be because the Si isotopic composition of diatoms ($\delta^{30}\mathrm{Si}_{\mathrm{BSi}}$) is lighter relative to seawater in which the diatoms grew, by approximately 1.1 ± 0.4 ‰ (s.d) (De La Rocha et al., 1997). The $\delta^{30}\mathrm{Si}_{\mathrm{BSi}}$ at the three sites along the WAP has been estimated from the $\delta^{30}\mathrm{Si}_{\mathrm{DSi}}$ of surface water, $\delta^{30}\mathrm{Si}_{\mathrm{DSi}}$ of initial water and the isotopic fractionation factor (ϵ) assuming the open-system model. Our observations suggest that the BSi produced in WAP surface waters would have a $\delta^{30}\mathrm{Si}_{\mathrm{BSi}}$ between −0.02 ‰ and +0.56 ‰ in the range of $\delta^{30}\mathrm{Si}_{\mathrm{BSi}}$ from fossil records along the WAP (Swann et al., 2017). In addition, lighter Si isotopes may also potentially be released during BSi dissolution (Demarest et al., 2009). Second, the precipitation of silica and/or formation of authigenic phases by reverse weathering is characterized by heavier $\delta^{30}\mathrm{Si}_{\mathrm{DSi\ pw}}$ (Ehlert et al., 2016; Geilert et al., 2014;

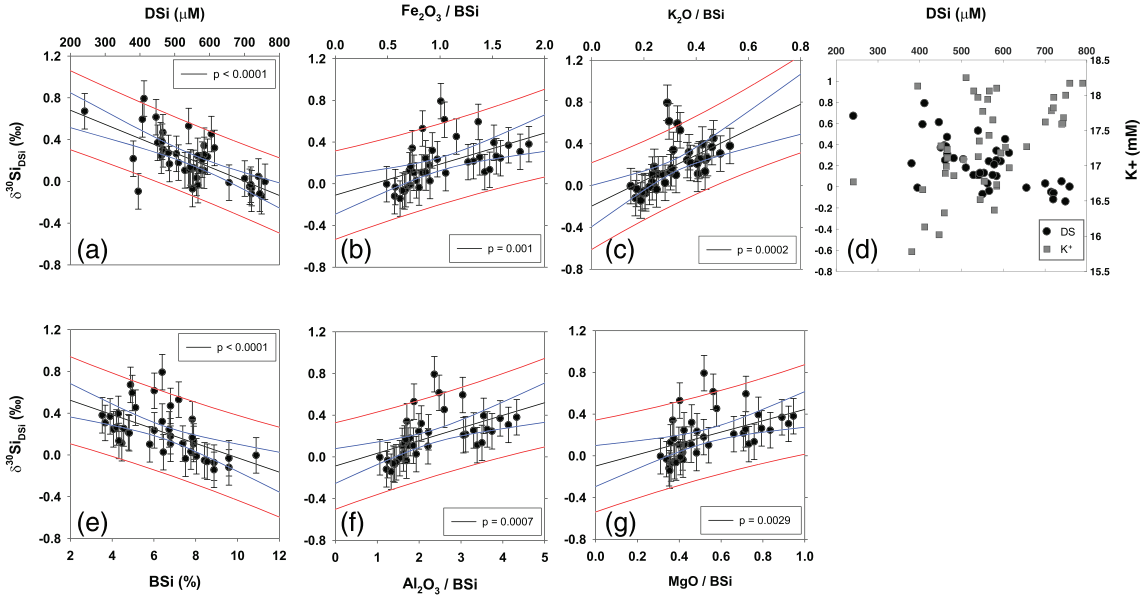

Figure 5. Silicon isotopes signature ($\delta^{30}Si_{DSi}$) of porewaters at all stations along the WAP plotted against silicic acid concentration (DSi) of the porewaters (a) and oxides present in major clay minerals (smectite, illite, chlorite, and kaolinite). (b) Iron oxide (Fe_2O_3), (c) potassium oxide (K_2O), (d) DSi and potassium cations (K^+), (e) biogenic silica (BSi), (f) aluminum oxide (Al_2O_3), and (g) magnesium oxide (MgO). All oxides are plotted relative to BSi to eliminate the influence of high BSi compared to oxide content. Black lines show best fit regression, blue lines = 95% confidence interval, and red lines = 95% prediction interval and the corresponding *p* value of each regression line.

Georg et al., 2009) and an increase in amorphous silica and/or solid phase of Al, Fe, K, and Mg (or a decrease in dissolved phase of Al, Fe, K, and Mg). Third, there is steady-state equilibrium with respect to Si between BSi dissolution and precipitation/weathering reactions, characterized by constant DSi concentration and $\delta^{30}Si_{DSi\ pw}$ with depth, with potentially also an increase in solid phases of Al, Fe, K, and Mg (decrease in dissolved phase of Al, Fe, K, and Mg).

The significant relationship between DSi, BSi, and diatom abundance (Figure 3) suggests that where more diatoms are present in the sediment there is more BSi dissolution supplying the porewater with DSi (assuming a constant dissolution behavior between stations), that is, that BSi dissolution is the primary driver of DSi release in the sediments (Scenario 1). The negative correlation between BSi and $\delta^{30}Si_{DSi\ pw}$ (Figure 5d) supports the assumption that the dissolution releases lighter isotopes into the surrounding porewaters. However, the positive correlation between $\delta^{30}Si_{DSi\ pw}$ and Al_2O_3, Fe_2O_3, MgO, and K_2O, and the negative correlation of DSi and K^+ with $\delta^{30}Si_{DSi\ pw}$, supports the scenario of weathering precipitating lighter Si isotopes (Scenario 2). This means that there is clearly both dynamic dissolution and reverse weathering reactions controlling DSi exchange within these WAP shelf sediments. Furthermore, the solubility of silica, described by the Al:DSi ratio of the porewater, shows an exponential relationship with $\delta^{30}Si_{DSi\ pw}$: the lower the solubility (high Al:DSi), the heavier $\delta^{30}Si_{DSi\ pw}$ (see SI), which is in accordance with the detrital:opal relationship previously observed (Aller, 2014; Bayon et al., 2018). The core-top waters show the highest Al:DSi ratio and the heaviest $\delta^{30}Si_{DSi\ pw}$, representing the location where early diagenetic dissolution/precipitation are likely to be most important (Tréguer & De La Rocha, 2013). Overall, our data show lighter $\delta^{30}Si_{DSi\ pw}$ than the bottom water and are enriched in light isotopes with depth, which suggest that despite the complex dynamics between the porewaters and their surrounding sediments, dissolution is the dominant factor controlling $\delta^{30}Si_{DSi\ pw}$.

4.1.4. Reaction-Transport Model to Disentangle the Reaction Network and Quantifying Benthic Fluxes

An inverse modeling approach using the Biogeochemical Reaction Network Simulator (BRNS) model is used here to infer the relative significance of BSi dissolution and authigenic precipitation on porewater DSi concentration, as well as the corresponding $\delta^{30}Si_{DSi}$ signature from the observational data, and to quantify benthic fluxes. The model setup considers a mass balance between transport processes and BSi dissolution, and the formation of authigenic phases controlling DSi and $\delta^{30}Si_{DSi}$ of the porewaters. Si isotopes are incorporated in the model setup assuming that the total abundance of Si isotopes is the sum of ^{28}Si and ^{30}Si and

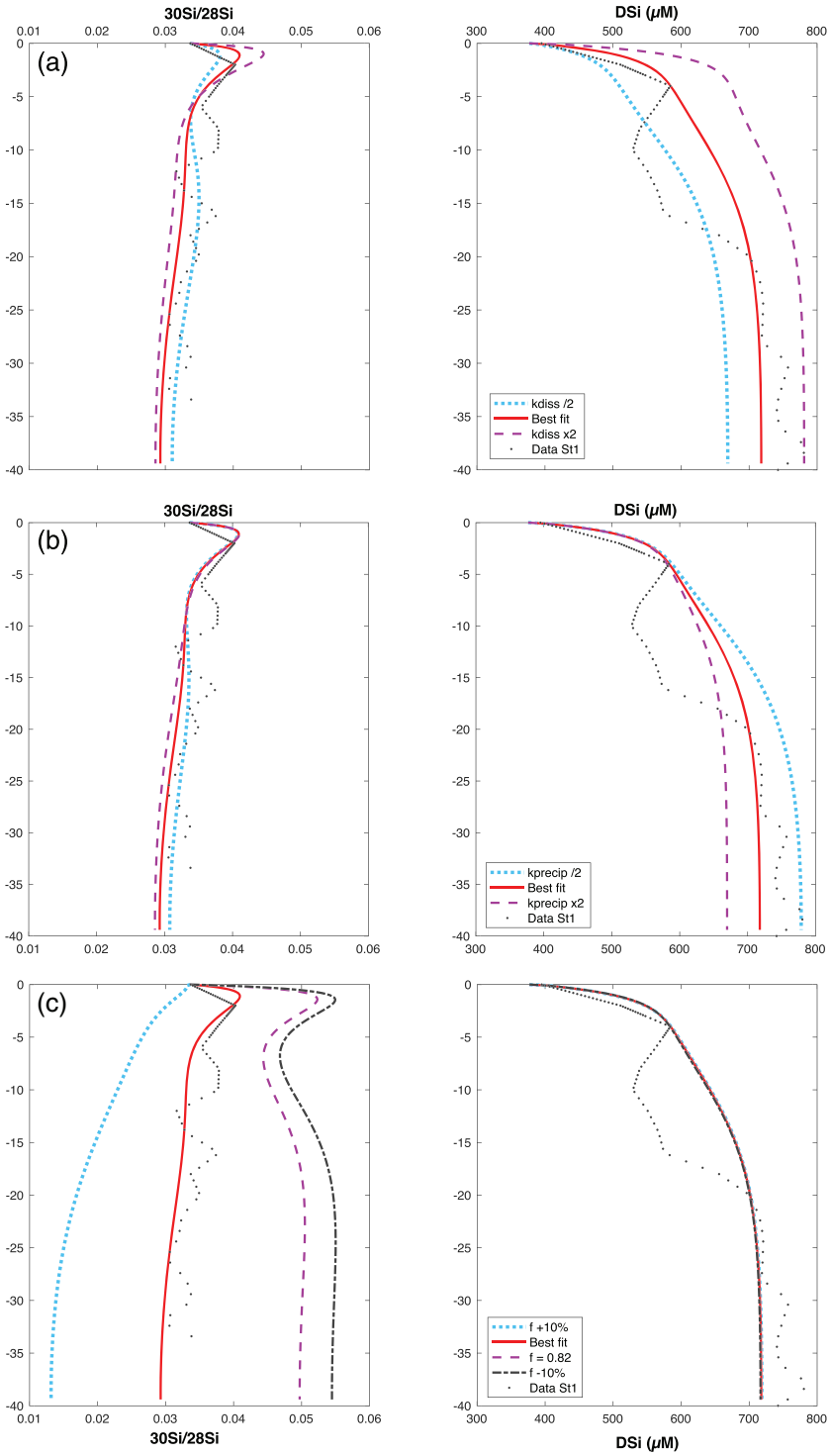

Figure 6. Sensitivity tests of silicic acid (DSi) concentration and $^{30}Si/^{28}Si$, at Station 1, in response to variation of single parameters from the best fit: (a) doubled or halved k_{diss} BSi rate constant of dissolution, (b) doubled or halved k_{precip}, molecular coefficient of precipitation, and (c) variation of 10% to DSi consumption in surface water ($f \pm 10\%$, where f is the fraction of initial DSi remaining in solution). $\delta^{30}Si_{BSi} = 0.24$ ‰ corresponds to $f = 0.82$ (calculated from this study), $\delta^{30}Si_{BSi} = 0.56$ ‰ corresponds to f-10%, $\delta^{30}Si_{BSi} = -0.65$ ‰ corresponds to f+10%. The best fit is achieved with a $\delta^{30}Si_{BSi} = -0.18$ ‰. Here, $^{30}Si/^{28}Si$ ratios are equivalent to $\delta^{30}Si_{DSi}$ considering that the total abundance of Si isotopes is the sum of ^{28}Si and ^{30}Si; see the SI for a conversion example.

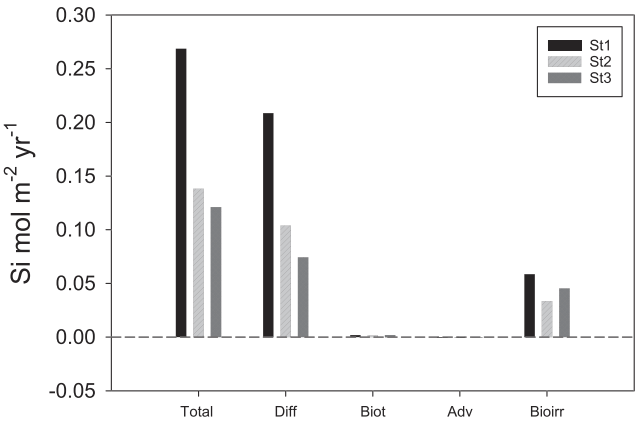

Figure 7. Total, diffusive, bioturbation, advective, and bioirrigation fluxes of Si calculated from the BRNS model best fit of St1 (black), St2 (light gray), and St3 (dark gray) along the WAP.

thus $\delta^{30}Si_{DSi}$ data have been converted to $^{28}Si/^{30}Si$ ratio for comparison (see the SI for a detailed model setup description and conversion example).

The reaction-transport model suggests that both DSi and $\delta^{30}Si_{DSi}$ are the combined result of biogenic silica dissolution and precipitation of authigenic silicate minerals. When the system is in steady state, porewaters reflect either Scenario 1 (dissolution dominates resulting in lighter $\delta^{30}Si_{DSi\ pw}$) or Scenario 2 (precipitation dominates resulting in heavier $\delta^{30}Si_{DSi\ pw}$) (Figures 6a and 6b). Because the system is not in steady state, especially at the surface (above 5–10 cm), the increase in heavy isotopes within the top of the core can be described by this imbalance where high dissolution induces high precipitation resulting in higher $\delta^{30}Si_{DSi\ pw}$. The dissolution rate of BSi is high, but the saturation of the porewater induces the rapid removal of Si through the precipitation of secondary minerals. This phenomenon is not reflected in the concentration profiles but does impact $\delta^{30}Si_{DSi\ pw}$ (Figure 6a).

The model includes a large number of fixed physical and biogeochemical parameters, molecular transport, and initial conditions. The best fit of both DSi and $\delta^{30}Si_{DSi}$ profiles presented in Figure 6 is the result of calculated and/or measured parameters such as the physical parameters: mixing rate and advection velocity, corrected porosity and measured salinity, and the molecular transport while biogeochemical parameters are mostly the results of the best fitting of the model to the data. All values are detailed in Table S6 in the SI. Model results show that the dissolution and precipitation coefficients (k_{diss} and k_{precip}), and the solubility of the authigenic phase (SA), decrease from St1 to St3. The value of k_{diss} is consistent with the sedimentation rate and the water depth of the core. St3 has the highest sedimentation rate and the shallowest water column depth, which allows for more highly reactive BSi to reach the sediment-water interface compared to station St1 and St2. Furthermore, the SA value agrees with the Al:DSi ratio where the Si solubility is higher at St1, which suggests that the precipitation of authigenic phases is less important at St1 compared to St2 and St3. The solubility gradient is supported by the north-south pattern of $\delta^{30}Si_{DSi\ pw}$, and SA values within the model are in accordance with the values described by Dixit et al. (2001). It is not possible to reproduce the BSi profiles, which is likely a limitation of the assumption of steady state. The BSi in the sediment will probably respond to short-term changes in export from bloom episodes happening in the surface waters. As such, a transient model would be required to capture the Si seasonal dynamics along the WAP. In addition, the $\delta^{30}Si_{DSi}$ of porewater is very sensitive to the BSi isotopic composition, which was estimated here and assumed to be constant. However, the isotopic composition of BSi could vary spatially and temporally on relatively short time scales (seasonal and bloom time scales). For example, if DSi uptake in surface water decreases (increases) by 10% (f −10%), $^{30}Si/^{28}Si$ ratio decreases (increases) by a factor of 4 (1.1) (Figure 6c). Our outputs from the model suggest that the BSi content deeper within the sediment is a relatively unreactive pool in accordance with low export and high recycling observed along the WAP (Stukel et al., 2015), which is consistent with the observed BSi profiles representing the variability of past export/productivity events. Overall, we suggest that benthic fluxes and surface sedimentary processes are likely to be sensitive to surface silica production and thus to the climatically driven changes in sea ice dynamics controlling phytoplanktonic blooms in the WAP area. Further investigations are required to fully understand the link between pelagic and benthic environments.

4.1.5. Simulated Benthic Fluxes

DSi in the porewater is supplied by BSi dissolution and/or other forms of Si sinking toward the sediment. The diffusive benthic fluxes calculated by Fick's law are very low (0.086 to 0.092 mol m^{-2} yr^{-1}), likely because the DSi concentration of bottom water is high relative to many regions in the oceans, reducing the concentration gradient to the porewater. Furthermore, our estimated fluxes are low because they merely take into consideration molecular diffusion and not other transport mechanisms, such as bioirrigation and bioturbation processes. Using the BRNS model, we are able to disentangle the relative contribution of burial, bioirrigation, and bioturbation to the total fluxes. Figure 7 shows the total and the contributions aforementioned to benthic fluxes for the three stations along the WAP.

Model-derived estimates of total Si fluxes decrease from north to south. Additionally, at all sites molecular diffusion is the dominant driver, which also agrees with estimated values based on core-top porewater

end-members, despite the caveats of such calculations. St3 shows a relatively high contribution from bioirrigation (Figure 7), which is in accordance with the presence of a large worm in the top 12 cm of the core. The gradient in total Si flux is in good agreement with the water depth. St1 is the deepest (589 m), located in the north part of the WAP, and shows the highest flux, which could be the result of the earlier sea ice retreat and thus possible dissolution of fresh sinking material to the surface sediment. In contrast, St2 and St3 show more similar total fluxes despite the difference in water depth (566 and 387 m, respectively), which could suggest that the fluxes at St2 and St3 represent the minimum Si benthic flux preceding the productive season.

5. Conclusion

This study presents seawater and porewater profiles of DSi and $\delta^{30}Si_{DSi}$ to evaluate for the first time the Si benthic fluxes along the WAP continental shelf. Additionally, we use $\delta^{30}Si_{DSi}$ of porewater ($\delta^{30}Si_{DSi\ pw}$) coupled with an integrated data-model approach to disentangle BSi dissolution and diagenetic processes as the source of benthic Si fluxes in the WAP region.

Our results highlight that the benthic DSi fluxes are dominated by the diffusive DSi flux and correspond to 26.7 ± 2.7 Gmol yr^{-1} (2 s.d.) for the WAP continental shelf area which is lower than flux estimates for continental slopes and most open Southern Ocean regions. Because our sampling occurred before the phytoplankton bloom, the calculated values are likely to represent the lower end of WAP DSi diffusive fluxes throughout the year. The results from the mass balance approach also show a low contribution of porewater to the bottom water and highlight a dynamic sediment-water interface with a loss of Si between the core-top water and the bottom water.

At all stations, $\delta^{30}Si_{DSi}$ is lower in porewater than in bottom water, indicating that dissolution is the dominant process supplying DSi in porewater. The DSi of the porewater does not always follow the typical asymptotic curve, suggesting that the system is not in equilibrium. We explored the source of DSi using $\delta^{30}Si_{DSi\ pw}$ within the context of three hypothetical scenarios. In Scenario (1) BSi dissolution dominates, increasing DSi porewater and enriching $\delta^{30}Si_{DSi\ pw}$ in ^{28}Si, in Scenario (2) authigenic formation dominates, decreasing DSi in the porewater and enriching $\delta^{30}Si_{DSi\ pw}$ in ^{30}Si, and in Scenario (3) dissolution and precipitation processes are balanced and thus DSi and $\delta^{30}Si_{DSi\ pw}$ show no variations. This simple approach is simulated with the BRNS model and shows that Si saturation plays a key role in dissolution-precipitation processes, especially in the top layer of the cores. It also shows that $\delta^{30}Si_{DSi\ pw}$ is sensitive to $\delta^{30}Si_{BSi}$.

Finally, both our observations and modeling suggest that the surface productivity could impact the benthic release of dissolved silicon but further investigations are required to understand the link between surface productivity and early diagenesis.

Data Availability Statement

An electronic copy of the diatom abundances, biogenic silica, silicic acid concentrations, and silicon isotope signatures data from this study is available online (at https://doi.pangaea.de/10.1594/PANGAEA.920055). XRF data are publicly available through the British Oceanographic Data Centre (BODC) (at https://doi.org/10.5285/b1282b1e-7852-5d16-e053-6c86abc04c61). Finally, physical parameters and the relevant referencing information are available at https://www.bodc.ac.uk/data/bodc_database/nodb/cruise/16039/, and finally water column and porewater nutrient, POM and isotopic data, and upper sediment data for the WAP shelf from cruise JR15003 are available at Henley et al. 2020 (https://doi.org/10.5285/b503dbdb-f954-4870-e053-6c86abc03f79).

Acknowledgments
We would like to thank the captain and crew of the RRS James Clark Ross. We also want to thank Dr. Pawel Gaca and Adam Cooper for the ^{210}Pb, with helpful input from Professors Andrew B. Cundy, Ian W. Croudace, and Phillip E. Warwick, and Dr. Jade E. Hatton for the BSi analyses. We also thank the two anonymous reviewers for their constructive comments. Data collection was funded by the UK Natural Environment Research Council (NERC) through the Collaborative Antarctic Science Scheme and by Royal Society grant RGF\EA\180068. S. F. H. was funded by the UK NERC grant NE/K010034/1, Y. L. F. was funded by NERC through ORCHESTRA (NE/N018095/1), F. S. F is funded by UKRI NERC through the Changing Arctic Ocean Programme (NE/P006493/1).

References

Aller, R. C. (2014). Sedimentary diagenesis, depositional environments, and benthic fluxes. In H. D. Holland & K. K. Turekian (Eds.), *Treatise on geochemistry: Second edition* (2nd ed., Vol. 8, pp. 293–334). Elsevier Ltd. https://doi.org/10.1016/B978-0-08-095975-7.00611-2

Annett, A. L., Henley, S. F., Venables, H. J., Meredith, M. P., Clarke, A., & Ganeshram, R. S. (2017). Silica cycling and isotopic composition in northern Marguerite Bay on the rapidly-warming western Antarctic Peninsula. *Deep-Sea Research Part II: Topical Studies in Oceanography*, *139*, 132–142. https://doi.org/10.1016/j.dsr2.2016.09.006

Appleby, P. G. (2008). Three decades of dating recent sediments by fallout radionuclides: A review. https://doi.org/10.1177/0959683607085598

Barnes, D. K. A. (2018). Blue carbon on polar and subpolar seabeds. In R. K. Agarwal (Ed.), *Carbon Capture, Utilization and Sequestration*. https://doi.org/10.5772/intechopen.78237

Baskaran, M. (2011). Po-210 and Pb-210 as atmospheric tracers and global atmospheric Pb-210 fallout: A Review. *Journal of Environmental Radioactivity*, *102*, 500–513. https://doi.org/10.1016/j.jenvrad.2010.10.007

Bayon, G., Delvigne, C., Ponzevera, E., Borges, A. V., Darchambeau, F., Deckker, P. D., & André, L. (2018). The silicon isotopic composition of fine-grained river sediments and its relation to climate and lithology. *Geochemica et Cosmochinica Acta*, *229*, 147–161. https://doi.org/10.1016/j.gca.2018.03.015

Berelson, W. M., Anderson, R. F., Dymond, J., DeMaster, D. J., Hammond, D. E., Collier, R., et al. (1997). Biogenic budgets of particle rain, benthic remineralization and sediment accumulation in the equatorial Pacific. *Deep-Sea Research Part II: Topical Studies in Oceanography*, *44*, 2251–2282. https://doi.org/10.1016/S0967-0645(97)00030-1

Boudreau, B. P. (1996). The diffusive tortuosity of fine-grained unlithified sediments. *Geochimica et Cosmochimica Acta*, *60*, 3139–3142. https://doi.org/10.1016/0016-7037(96)00158-5

Brearley, J. A., Meredith, M. P., Naveira Garabato, A. C., Venables, H. J., & Inall, M. E. (2017). Controls on turbulent mixing on the West Antarctic Peninsula shelf. *Deep-Sea Research Part II: Topical Studies in Oceanography*, *139*, 18–30. https://doi.org/10.1016/j.dsr2.2017.02.011

Brown, K. M., & Ransom, B. (1996). Porosity corrections of smectite-rich sediments: Impact on studies of compaction, fluid generation, and tectonic history. *Geology*, *24*, 843–846.

Buesseler, K. O., McDonnell, A. M. P., Schofield, O. M. E., Steinberg, D. K., & Ducklow, H. W. (2010). High particle export over the continental shelf of the west Antarctic Peninsula. *Geophysical Research Letters*, *37*, L22606. https://doi.org/10.1029/2010GL045448

Cardinal, D., Alleman, L. Y., de Jong, J., Ziegler, K., & Andre, L. (2003). Isotopic composition of silicon measured by multicollector plasma source mass spectrometry in dry plasma mode. *Journal of Analytical Atomic Spectrometry*, *18*, 213–218. https://doi.org/10.1039/b210109b

Cassarino, L., Hendry, K. R., Meredith, M. P., Venables, H. J., & De La Rocha, C. L. (2017). Silicon isotope and silicic acid uptake in surface waters of Marguerite Bay, West Antarctic Peninsula. *Deep-Sea Research Part II: Topical Studies in Oceanography*, *139*, 143–150. https://doi.org/10.1016/j.dsr2.2016.11.002

Clarke, A., Meredith, M. P., Wallace, M. I., Brandon, M. A., & Thomas, D. N. (2008). Seasonal and interannual variability in temperature, chlorophyll and macronutrients in northern Marguerite Bay, Antarctica. *Deep-Sea Research Part II: Topical Studies in Oceanography*, *55*, 1988–2006. https://doi.org/10.1016/j.dsr2.2008.04.035

Couto, N., Martinson, D. G., Kohut, J., & Schofield, O. (2017). Distribution of Upper Circumpolar Deep Water on the warming continental shelf of the West Antarctic Peninsula. *Journal of Geophysical Research: Oceans*, *122*, 5306–5315. https://doi.org/10.1002/2017JC012840

De La Rocha, C. L., Brzezinski, M. A., & Deniro, M. J. (1997). Fractionation of silicon isotopes by marine diatoms during biogenic silica formation. *Geochimica Et Cosmochimica Acta*, *61*, 5051–5056. https://doi.org/10.1016/S0016-7037(97)00300-1

DeMaster, D. J. (1981). The supply and accumulation of silica in the marine environment. *Geochimica et Cosmochimica Acta*, *45*(10), 1715–1732. https://doi.org/10.1016/0016-7037(81)90006-5

DeMaster, D. J. (2013). The diagenesis of biogenic silica: Chemical transformations occurring in the water column, seabed, and crust. *Treatise on geochemistry: Second edition* (2nd ed., Vol. 9, pp. 103–111). Elsevier Ltd. https://doi.org/10.1016/B978-0-08-095975-7.00704-X

DeMaster, D. J., Ragueneau, O. G., & Nittrouer, C. (1996). Preservation efficiencies and accumulation rates of biogenic silica and organic C, N, and P in high-latitude sediments: The Ross Sea. *Journal of Geophysical Research*, *101*, 18,501–18,518.

Demarest, M. S., Brzezinski, M. A., & Beucher, C. P. (2009). Fractionation of silicon isotopes during biogenic silica dissolution. *Geochimica et Cosmochimica Acta*, *73*, 5572–5583. https://doi.org/10.1016/0016-7037(81)90006-5

Dixit, S., Van Cappellen, P., & van Bennekom, J. (2001). Processes controllong solubility of biogenic silica and pore water build-up of silicic acid in marine sediments. *Marine Chemistry*, *73*, 333–352.

Ducklow, H. W., Clarke, A., Dickhut, R., Doney, S. C., Geisz, H., Huang, K., et al. (2012). The marine system of the Western Antarctic Peninsula. Antarctic Ecosystems: An Extreme Environment in a Changing World, 121–159.

Ehlert, C., Doering, K., Wallmann, K., Scholz, F., Sommer, S., Grasse, P., et al.(2016). Stable silicon isotope signatures of marine pore waters—Biogenic opal dissolution versus authigenic clay mineral formation. *Geochimica et Cosmochimica Acta*, *191*, 102–117. https://doi.org/10.1016/j.gca.2016.07.022

Fripiat, F., Cavagna, A. J., Savoye, N., Dehairs, F., Andre, L., & Cardinal, D. (2011). Isotopic constraints on the Si-biogeochemical cycle of the Antarctic Zone in the Kerguelen area (KEOPS). *Marine Chemistry*, *123*, 11–22. https://doi.org/10.1016/j.marchem.2010.08.005

Geilert, S., Grasse, P., Doering, K., Wallmann, K., Ehlert, C., Sholz, F., & Hensen, C. (2020). Impact of ambient conditions on the Si isotope fractionation in marine pore fluids during early diagenesis. *Biogeosciences*, *17*, 1745–1763. https://doi.org/10.5194/bg-17-1745-2020

Geilert, S., Vroon, P. Z., Roerdink, D. L., Van Cappellen, P., & van Bergen, M. J. (2014). Silicon isotope fractionation during abiotic silica precipitation at low temperatures : Inferences from flow-through experiments. *Geochimica et Cosmochimica Acta*, *142*, 95–114. https://doi.org/10.1016/j.gca.2014.07.003

Georg, R. B., Zhu, C., Reynolds, B. C., & Halliday, A. N. (2009). Stable silicon isotopes of groundwater, feldspars, and clay coatings in the Navajo Sandstone aquifer, Black Mesa, Arizona, USA. *Geochimica et Cosmochimica Acta*, *73*, 2229–2241. https://doi.org/10.1016/j.gca.2009.02.005

Govindaraju, K. (1994). Compilation of working values and sample description for geostandards. *Geostandards Newsletter*, *18*, 1–158. https://doi.org/10.1046/j.1365-2494.1998.53202081.x-i1

Grasse, P., Brzezinski, M. A., Cardinal, D., de Souza, G. F., Andersson, P. S., Closset, I., et al. (2017). GEOTRACES inter-calibration of the stable silicon isotope composition of dissolved silicic acid in seawater. *Journal of Analytical Atomic Spectrometry*, *32*, 562–578. https://doi.org/10.1039/C6JA00302H

Hawkings, J. R., Wadham, J. L., Benning, L. G., Hendry, K. R., Tranter, M., Tedstone, A., et al. (2017). Ice sheets as a missing source of silica to the polar oceans. *Nature Communications*, *8*, 14198. https://doi.org/10.1038/ncomms14198

Hendry, K. R., Georg, B. R., Rickaby, R. E. M., Robinson, L. F., & Halliday, A. N. (2010). Deep ocean nutrients during the Last Glacial Maximum deduced from sponge silicon isotopic compositions. *Earth and Planetary Science Letters*, *292*, 290–300. https://doi.org/10.1016/j.epsl.2010.02.005

Hendry, K. R., Leng, M. J., Robinson, L. F., Sloane, H. J., Blusztjan, J., Rickaby, R. E. M., et al. (2011). Silicon isotopes in Antarctic sponges: An interlaboratory comparison. *Antarctic Science*, *23*, 34–42. https://doi.org/10.1017/S0954102010000593

Hendry, K. R., Meredith, M. P., Measures, C. I., Carson, D. S., & Rickaby, R. E. M. (2010). The role of sea ice formation in cycling of aluminium in northern Marguerite Bay, Antarctica. *Estuarine, Coastal and Shelf Science*, *87*, 103–112. https://doi.org/10.1016/j.ecss.2009.12.017

Henley, S. F., Jones, E. M., Venables, H. J., Meredith, M. P., Firing, Y. L., Dittrich, R., et al. (2018). Macronutrient and carbon supply, uptake and cycling across the Antarctic Peninsula shelf during summer. *Philosophical Transactions of the Royal Society A: Mathematical, Physical and Engineering Sciences*, *376*, 1–28. https://doi.org/10.1098/rsta.2017.0168

Henley, S. F., Schofield, O. M. E., Hendry, K. R., Schloss, I. R., Steinberg, D. K., Moffat, C., & Meredith, M. P. (2019). Variability and change in the west Antarctic Peninsula marine system : Research priorities and opportunities. *Progress in Oceanography*, *173*, 208–237. https://doi.org/10.1016/j.pocean.2019.03.003

Hobbs, W. R., Massom, R., Stammerjohn, S., Reid, P., Williams, G., & Meier, W. (2016). A review of recent changes in Southern Ocean sea ice, their drivers and forcings. *Global and Planetary Change*, *143*, 228–250. https://doi.org/10.1016/j.gloplacha.2016.06.008

Karl, D. M., & Tien, G. (1992). MAGIC: A sensitive and precise method for measuring dissolved phosphorus in aquatic environments. *Limnology and Oceanography*, *37*, 105–116. https://doi.org/10.4319/lo.1992.37.1.0105

Kavanaugh, M. T., Abdala, F. N., Ducklow, H., Glover, D., Fraser, W., Martinson, D., et al. (2015). Effect of continental shelf canyons on phytoplankton biomass and community composition along the western Antarctic Peninsula. *Marine Ecology Progress Series*, *524*(Vaughan 2006), 11–26. https://doi.org/10.3354/meps11189

Kohut, J. T., Winsor, P., Statscewich, H., Oliver, M. J., Fredj, E., Couto, N., et al. (2018). Variability in summer surface residence time within a West Antarctic Peninsula biological hotspot. *Philosophical Transactions of the Royal Society A: Mathematical, Physical and Engineering Sciences*, *376*, 1–13. https://doi.org/10.1098/rsta.2017.0165

Koning, E., Brummer, G. J., Van Raaphorst, W., Van Bennekom, J., Helder, W., & Van Iperen, J. (1997). Settling, dissolution and burial of biogenic silica in the sediments off Somalia (northwestern Indian Ocean). *Deep-Sea Research Part II: Topical Studies in Oceanography*, *44*, 1341–1360. https://doi.org/10.1016/S0967-0645(97)00018-0

Martinson, D. G., & McKee, D. C. (2012). Transport of warm upper circumpolar deep water onto the Western Antarctic Peninsula Continental Shelf. *Ocean Science*, *8*(4), 433–442. https://doi.org/10.5194/os-8-433-2012

Martinson, D. G., Stammerjohn, S. E., Iannuzzi, R. A., Smith, R. C., & Vernet, M. (2008). Western Antarctic Peninsula physical oceanography and spatio-temporal variability. *Deep Sea Research Part II: Topical Studies in Oceanography*, *55*(18–19), 1964–1987. https://doi.org/10.1016/j.dsr2.2008.04.038

McManus, J., Hammond, D. E., Berelson, W. M., Kilgore, T. E., Demaster, D. J., Ragueneau, O. G., & Collier, R. W. (1995). Early diagenesis of biogenic opal: Dissolution rates, kinetics, and paleoceanographic implications. *Deep Sea Research Part II: Topical Studies in Oceanography*, *42*(2–3), 871–903.

Meredith, M. P., Stefels, J., & van Leeuwe, M. (2017). Marine studies at the western Antarctic Peninsula: Priorities, progress and prognosis. *Deep-Sea Research Part II: Topical Studies in Oceanography*, *139*, 1–8. https://doi.org/10.1016/j.dsr2.2017.02.002

Moffat, C., & Meredith, M. (2018). Shelf-ocean exchange and hydrography west of the Antarctic Peninsula: A review. *Philosophical Transactions of the Royal Society A: Mathematical, Physical and Engineering Sciences*, *376*, 1–17. https://doi.org/10.1098/rsta.2017.0164

Norrish, K., & Hutton, J. T. (1969). An accurate X-ray spectrographic method for the analysis of a wide range of geological samples. *Geochimica et Cosmochimica Acta*, *33*(4), 431–453. https://doi.org/10.1016/0016-7037(69)90126-4

Orsi, A. H., Whitworth, T. III, & Nowlin, W. D. Jr. (1995). On the meridional extent and fronts of the Antarctic Circumpolar Current. *Deep Sea Research*, *42*, 641–673. https://doi.org/10.1016/0967-0637(95)00021-W

Pondaven, P., Ragueneau, O., Tréguer, P., Hauvespre, A., Dezileau, L., & Reyss, J. L. (2000). Resolving the pal paradox' in the Southern Ocean. *Nature*, *405*(6783), 168–172.

Rabouille, C., Gaillard, J. F., Tréguer, P., & Vincendeau, M. A. (1997). Biogenic silica recycling in surficial sediments across the Polar Front of the Southern Ocean (Indian Sector). *Deep-Sea Research Part II: Topical Studies in Oceanography*, *44*, 1151–1176. https://doi.org/10.1016/S0967-0645(96)00108-7

Ragueneau, O., Gallinari, M., Corrin, L., Grandel, S., Hall, P., Hauvespre, A., et al. (2001). The benthic silica cycle in the Northeast Atlantic: Annual mass balance, seasonality, and importance of non-steady-state processes for the early diagenesis of biogenic opal in deep-sea sediments. *Progress in Oceanography*, *50*(1–4), 171–200.

Ragueneau, O., Regaudie-de Gioux, A., Moriceau, B., Gallinari, M., Vangriesheim, A., Baurand, F., & Khripounoff, A. (2009). A benthic Si mass balance on the Congo margin: Origin of the 4000 m DSi anomaly and implications for the transfer of Si from land to ocean. *Deep Sea Research Part II: Topical Studies in Oceanography*, *56*(23), 2197–2207.

Ragueneau, O., Tréguer, P., Leynaert, A., Anderson, R. F., Brzezinski, M. A., DeMaster, D. J., et al. (2000). A review of the Si cycle in the modern ocean: Recent progress and missing gaps in the application of biogenic opal as a paleoproductivity proxy. *Global and Planetary Change*, *26*(4), 317–365.

Rebreanu, L., Vanderborght, J.-P., & Chou, L. (2008). The diffusion coefficient of dissolved silica revisited. *Marine Chemistry*, *112*, 230–233. https://doi.org/10.1016/j.marchem.2008.08.004

Reynolds, B. C., Frank, M., & Halliday, A. N. (2006). Silicon isotope fractionation during nutrient utilization in the North Pacific. *Earth and Planetary Science Letters*, *244*, 431–443. https://doi.org/10.1016/j.epsl.2006.02.002

San Miguel, E. G., Pérez-Moreno, J. P., Bolívar, J. P., García-Tenorio, R., & Martin, J. E. (2002). ^{210}Pb determination by gamma spectrometry in voluminal samples (cylindrical geometry). *Nuclear Instruments and Methods in Physics Research, Section A: Accelerators, Spectrometers, Detectors and Associated Equipment*, *493*, 111–120. https://doi.org/10.1016/S0168-9002(02)01415-8

Sayles, F. L., Deuser, W. G., Goudreau, J. E., Dickinson, W. H., Jickells, T. D., & King, P. (1996). The benthic cycle of biogenic opal at the Bermuda Atlantic Time Series site. *Deep-Sea Research Part I: Oceanographic Research Papers*, *43*, 383–409. https://doi.org/10.1016/0967-0637(96)00027-1

Scherer, R. P. (1994). A new method for the determination of absolute abundance of diatoms and other silt-sized sedimentary particles. *Journal of Paleolimology*, *12*, 171–179.

Schofield, O., Ducklow, H., Bernard, K., Doney, S., Patterson-Fraser, D., Gorman, K., et al. (2013). Penguin biogeography along the West Antarctic Peninsula: Testing the canyon hypothesis with Palmer LTER Observations. *Oceanography*, *26*(3), 204–206. https://doi.org/10.5670/oceanog.2013.63

Schrader, H. J., & Gersonde, R. (1978). Diatoms and silicoflagellates. Micropaleontological counting methods and techniques: An exercise on an 8 m section of the lower Pliocene of Capo Rossello, Sicily. *Utrecht Micropaleontology Bulletin*, *17*, 129–176.

Schulz, H. D., & Zabel, M. (Eds.) (2006). *Marine geochemistry* (2nd revise). Springer. https://doi.org/10.1007/3-540-32144-6

Smith, R. C., Ainley, D., Baker, K., Domack, E., Emslie, S., Fraser, B., et al. (1999). Marine ecosystem sensitivity to climate change: Historical observations and paleoecological records reveal ecological transitions in the Antarctic Peninsula region. *Bioscience*, *49*, 393–404. https://doi.org/10.2307/1313632

Strickland, J. D. H., & Parsons, T. R. (1972). *A practical handbook of seawater analysis* (2nd ed.). Canada: Fisheries Research Board of Canada.

Stukel, M. R., Asher, E., Couto, N., Schofield, O., Strebel, S., Tortell, P., & Ducklow, H. W. (2015). The imbalance of new and export production in the western Antractic Peninsula, a potentially "leaky" ecosystem. *Global Biogeochemical Cycles*, *29*, 1400–1420. https://doi.org/10.1002/2015GB005211

Swann, G. E. A., Pike, J., Leng, M. J., Sloane, H. J., & Snelling, A. M. (2017). Temporal controls on silicic acid utilisation along the West Antarctic Peninsula. *Nature Publishing Group*, *8*, 1–8. https://doi.org/10.1038/ncomms14645

Tréguer, P., & De La Rocha, C. L. (2013). The world ocean silica cycle. *Annual Review of Marine Science*, *5*(1), 477–501. https://doi.org/10.1146/annurev-marine-121211-172346

Turner, J., Lu, H., White, I., King, J. C., Phillips, T., Hosking, J. S., et al. (2016). Absence of 21st century warming on Antarctic Peninsula consistent with natural variability. *Nature*, *535*, 411–415. https://doi.org/10.1038/nature18645

Van Cappellen, P., & Qiu, L. (1997). Biogenic silica dissolution in sediments of the Southern Ocean. I. Solubility. *Deep-Sea Research Part II: Topical Studies in Oceanography*, *44*, 1109–1128. https://doi.org/10.1016/S0967-0645(96)00113-0

Venables, H. J., Clarke, A., & Meredith, M. P. (2013). Wintertime controls on summer stratification and productivity at the western Antarctic Peninsula. *Limnology and Oceanography*, *58*, 1035–1047. https://doi.org/10.4319/lo.2013.58.3.1035

Venables, H. J., Meredith, M. P., & Brearley, J. A. (2017). Modification of deep waters in Marguerite Bay, western Antarctic Peninsula, caused by topographic overflows. *Deep-Sea Research Part II: Topical Studies in Oceanography*, *139*, 9–17. https://doi.org/10.1016/j.dsr2.2016.09.005

Volpi, V., Camerlenghi, A., Hillenbrand, C. D., Rebesco, M., & Ivaldi, R. (2003). Effects of biogenic silica on sediment compaction and slope stability on the Pacific margin of the Antarctic Peninsula. *Basin Research*, *15*(3), 339–363. https://doi.org/10.1046/j.1365-2117.2003.00210.x

Wallace, M. I., Meredith, M. P., Brandon, M. A., Sherwin, T. J., Dale, A., & Clarke, A. (2008). On the characteristics of internal tides and coastal upwelling behaviour in Marguerite Bay, west Antarctic Peninsula. *Deep-Sea Research Part Ii-Topical Studies in Oceanography*, *55*, 2023–2040. https://doi.org/10.1016/j.dsr2.2008.04.033

Wetzel, F., de Souza, G. F., & Reynolds, B. C. (2014). What controls silicon isotope fractionation during dissolution of diatom opal? *Geochimica et Cosmochimica Acta*, *131*, 128–137. https://doi.org/10.1016/j.gca.2014.01.028

Ziegler, K., Chadwick, O. A., Brzezinski, M. A., & Kelly, E. F. (2005). Natural variations of δ^{30}Si ratios during progressive basalt weathering, Hawaiian Islands. *Geochimica et Cosmochimica Acta*, *69*, 4597–4610. https://doi.org/10.1016/j.gca.2005.05.008